Stationary External Rossby Waves in Vertical Shear

ISAAC M. HELD

Geophysical Fluid Dynamics Laboratory/NOAA, Princeton University, Princeton, NJ 08540

R. LEE PANETTA

Geophysical Fluid Dynamics Program, Princeton University, Princeton, NJ 08540

RAYMOND T. PIERREHUMBERT

Geophysical Fluid Dynamics Laboratory/NOAA, Princeton University, Princeton, NJ 08540

(Manuscript received 20 August 1984, in final form 11 December 1984)

ABSTRACT

The structure of stationary Rossby waves in the presence of a mean westerly zonal flow with vertical shear is examined. There is typically only one stationary vertical mode, the external mode, trapped within the troposphere. For more than one tropospheric mode to exist, we find that vertical shears must be smaller than those usually observed in extratropical latitudes. The vertical structure, horizontal wavenumber and group velocity of the external mode, and the projection onto this mode of topographic and thermal forcing are studied with continuous models (a linear shear profile as well as more realistic basic states), and a finite-differenced model with resolution and upper boundary condition similar to that used in GCMs. We point out that the rigid-lid upper boundary condition need not create artificial stationary resonances, as the artificial stationary vertical modes that are created are often horizontally evanescent.

The results are presented in a form which allows one to design the equivalent barotropic model that captures the external mode's contribution to the stationary wave field. It is found, in particular, that the wind blowing over the topography in such a barotropic model should generally be larger than the surface wind but smaller than the wind at the equivalent barotropic level. Also, the group velocity of the stationary external mode in realistic vertical shear is found to be considerably greater than that of the stationary Rossby wave in the equivalent barotropic model.

1. Introduction

The barotropic vorticity equation has played a central role in the historical development of our understanding of stationary planetary waves forced by topography, the seminal work being the beta-plane analysis of Charney and Eliassen (1949). More recently, it has been found that the barotropic vorticity equation on a sphere, linearized about an upper tropospheric zonal flow, can yield surprisingly realistic tropospheric stationary wave patterns (e.g., Grose and Hoskins, 1979; Held, 1983). Furthermore, it appears that for particular choices of the strength of the topographic forcing and the level of the zonal flow about which one linearizes in the barotropic model, a good fit to baroclinic stationary wave calculations can be obtained in the extratropical troposphere (compare Fig. 8 in Hoskins and Karoly, 1981, with Fig. 4 in Grose and Hoskins, 1979). Barotropic models have also been used to study the midlatitude responses to subtropical thermal forcing, and baroclinic models once again seem to confirm the value of the barotropic calculations (Simmons, 1982; Hoskins and Karoly, 1981).

The extent to which the extratropical stationary wave pattern is equivalent barotropic is well illustrated in Wallace (1983). The midlatitudes of the Southern Hemisphere (Wallace, Figs. 2.15 and 2.19) are clearly dominated by an equivalent barotropic structure, with maximum geopotential amplitude near the tropopause and small amplitude near the surface. This structure also stands out very clearly in Fig. 1 of Randel and Stanford (1983). A very similar structure is apparent in the Northern Hemisphere (see Wallace, Figs. 2.3 and 2.8) but is not quite as dominant, due to propagation into the stratosphere at high latitudes in winter and monsoonal flows in middle and subtropical latitudes in summer. It has also been demonstrated that much of the low-frequency variability in the Northern Hemisphere extratropical troposphere during winter is equivalent barotropic, particularly over the oceans, and also has maximum geopotential amplitude near the tropopause (e.g., Blackmon *et al.*, 1979). The wavelike teleconnection patterns, most notably the "PNA" pattern, have this vertical structure, as well as a horizontal structure strikingly similar to that of stationary barotropic Rossby waves (Namais, 1978; Wallace and Gutzler, 1981; Dole, 1983).

Localized orographic or stationary thermal forcing in extratropical latitudes generates a spectrum of planetary waves. Those with larger horizontal scales propagate into the stratosphere (in winter); those with smaller scales are trapped in a waveguide between the ground and upper-tropospheric westerlies. These trapped waves decay as they travel downstream, due to destructive interference between upward- and downward-propagating waves, except for the vertical modes supported by the waveguide. When $\bar{u}$ is assumed to be horizontally uniform and is given a vertical structure similar to that of the observed midlatitude winds, vertical modes do exist with vertical structure $A(p)$ closely resembling that observed (Held, 1983). These solutions are the familiar external Rossby waves, or planetary edge waves (Lindzen, 1967), strongly modified by vertical shear in the mean flow. Where this external mode dominates, the flow will be separable, $\psi' = A(p)\Psi(x, y)$, as postulated in derivations of equivalent barotropic models. [Strictly speaking, in the standard derivation of an equivalent barotropic model (Charney and Eliassen, 1949; Holton, 1979) one assumes that the total geostrophic streamfunction is separable. In the context of linear stationary wave theory, one need only assume that the deviations from zonal symmetry are separable.]

If the basic state flow is not horizontally uniform, separable solutions to the homogeneous problem will not exist in general. However, if the mean flow variations are sufficiently slow, external Rossby wavetrain solutions will exist with slowly varying vertical structure $A(p; x, y)$ determined by the structure of the external mode on the local mean flow. The path of the stationary wavetrain can be determined by ray tracing as in Hoskins and Karoly (1981), but using the local dispersion relation for the external mode rather than that for nondivergent Rossby waves. The picture that emerges is that observed stationary and low-frequency equivalent barotropic structures are, at least in part, external Rossby wavetrains generated by remote forcing, with local vertical structure controlled by the vertical structure of the basic state through which the wavetrains propagate.

The structure of stationary Rossby waves in a semi-infinite atmosphere with vertical shear has been examined by Tung and Lindzen (1979) and Plumb (1981), although emphasis in both of these papers is placed on modes whose existence is due to the mesospheric polar night jet. Geisler and Dickinson (1975) discuss the neutral modes in Charney's model and in models with more realistic vertical structures, but are concerned primarily with the effects of the non-Doppler term in the lower boundary condition for transient waves and with the relationship between the neutral and unstable modes. The rather different problems associated with the fast westward-propagating external Rossby waves, which are only slightly affected by tropospheric winds, have received more attention (Geisler and Dickinson, 1975; Salby, 1981). In this paper we focus on the structure and excitation of stationary external Rossby waves in the presence of a basic flow that is a function of height only and that is everywhere westerly.

It is convenient to think of the stationary external Rossby wave as one member of a complete orthonormal set of vertical modes. One can then simply project the forcing onto the mode of interest and derive the appropriate horizontal structure equation. In a semi-infinite atmosphere, this complete set of vertical modes consists of discrete and continuous parts, the individual modes in the continuous spectrum being "scattering states" that do not individually satisfy a radiation condition as $z \to \infty$. This vertical modal description is presented in Sections 2a and b. As it is infrequently used in meteorology, in Section 2c we compare this description with the more common approach (decomposition in longitudinal Fourier modes, followed by solution of a latitude–height structure equation for each mode) for the special case of a constant zonal flow. Some general properties of the external mode in vertical shear are described in 2d and e. In Sections 3 and 4 we discuss, for different mean flows, the number of discrete modes with wavelike (rather than evanescent) horizontal structure, and the vertical structure and group velocity of the external mode. Charney's model is analyzed in Section 3, and somewhat more complex, but still idealized, basic states with bounded winds and a tropopause in Section 4. In each case, we show how to design an equivalent barotropic model that reproduces the correct response where the external mode dominates. Charney's model is attractive in that simple analytic results for the vertical structure, equivalent barotropic height, etc., are available in the interesting limit of small surface winds. The numerical results of Section 4 are useful for examining the consequences in Charney's model of the unrealistic unbounded mean winds and the absence of a tropopause. Section 5 contains a local analysis of the external mode's structure and group velocity as a function of latitude using observed zonal winds and using vertical resolution and an upper boundary condition typical of that in GCMs. This calculation provides somewhat more quantitative information on the stationary external mode in the atmosphere.

2. Vertical modal decomposition for stationary waves

a. Basic equations and notation

The thermodynamic and vorticity equations for stationary quasi-geostrophic waves on a beta-plane of infinite horizontal extent, forced by topography h and heating per unit mass Q, and linearized about a horizontally uniform zonal flow $\bar{u}(z)$, can be written in the form

$$\bar{u}\partial_z v' - v'\partial_z \bar{u} + N^2 f_0^{-1} w' = \kappa Q/(f_0 H),$$

$$\bar{u}\nabla^2 v' + \beta v' = f_0 \rho_0^{-1}\partial_z(\rho_0 w'), \quad (2.1)$$

with the surface boundary condition obtained by setting $w' = \bar{u}\partial_x h$ at $z = 0$,

$$\bar{u}\partial_z v' - v'\partial_z \bar{u} = \kappa Q/(f_0 H) - N^2 f_0^{-1}\bar{u}\partial_x h. \quad (2.1')$$

We use $z \equiv H \ln(p_*/p)$ as vertical coordinate, where $H \equiv RT(0)/g$. Also, $\rho_0 \equiv e^{-z/H}$, $N^2 \equiv RH^{-1}(\partial_z T + \kappa T/H)$, $\kappa \equiv R/c_p$, and $v' = \partial_x \psi'$, where ψ' is the eddy geostrophic streamfunction. The notation is otherwise standard. The potential vorticity equation obtained from (2.1) reads

$$\bar{u}[\nabla^2 v' + f_0^2 \rho_0^{-1}\partial_z(\rho_0 N^{-2}\partial_z v')] + \bar{q}_y v' = \kappa f_0 \partial_z(\rho_0 N^{-2} Q)/(\rho_0 H) \quad (2.2)$$

where $\bar{q}_y \equiv \beta - f_0^2 \rho_0^{-1}\partial_z(\rho_0 N^{-2}\partial_z \bar{u})$. It is assumed throughout that $\bar{u} > 0$ for all z.

One can solve for the forced waves by first performing a modal decomposition in the vertical. Such a decomposition is common in oceanography, where the domain is finite in z, leading to a standard Sturm–Liouville eigenvalue problem for the vertical modes. It is less common in meteorology, since the semi-infinite domain causes the complete set of vertical modes to consist of both discrete trapped modes ("bound states") and continuum modes ("scattering states"). Despite this complication, a modal decomposition remains useful when one or a small number of modes dominate the solution in some region (e.g., Gill, 1983, p. 176; or Friedman, 1966).

The relevant eigenvalue problem is

$$f_0^2 \rho_0^{-1}\partial_z(\rho_0 N^{-2}\partial_z v_\alpha) + \bar{u}^{-1}\bar{q}_y v_\alpha = -\lambda_\alpha v_\alpha, \quad z \geq 0, \quad (2.3)$$

$$\partial_z v_\alpha - v_\alpha \bar{u}^{-1}\partial_z \bar{u} = 0, \quad z = 0.$$

Modes in the discrete spectrum are required to be evanescent at infinity, $\rho_0^{1/2} v_\alpha \to 0$ as $z \to \infty$; for the continuum modes, $\rho_0^{1/2} v_\alpha$ is bounded at infinity. Equation (2.3) is self-adjoint under the inner product

$$\langle A, B\rangle \equiv H^{-1}\int_0^\infty \rho_0 AB dz.$$

Therefore, all eigenvalues λ_α are real, and the eigenfunctions when suitably normalized satisfy

$$\langle v_\alpha, v_\beta\rangle = \delta_{\alpha\beta}, \quad (2.4)$$

where the rhs of (2.4) should be interpreted as the Dirac δ-function, $\delta(\alpha - \beta)$, for two eigenfunctions in the continuous spectrum. Vertical velocities associated with a particular mode can be obtained from either the thermodynamic or vorticity equations:

$$\bar{u}\partial_z v_\alpha - v_\alpha \partial_z \bar{u} = -N^2 f_0^{-1} w_\alpha, \quad (2.5a)$$

$$(\bar{u}\lambda_\alpha + \beta)v_\alpha = f_0 \rho_0^{-1}\partial_z(\rho_0 w_\alpha). \quad (2.5b)$$

b. Horizontal structure equation and equivalent barotropic models

The eigenmodes of (2.3) form a complete set, so the vertical profile of the forced wave at each point (x, y) can be expanded in terms of the $\{v_\alpha\}$. In order to solve for the forced wave we need only determine the horizontally dependent coefficient with which each v_α appears in the expansion. After rewriting (2.3) as $Lv_\alpha = -\lambda_\alpha v_\alpha$, one can show, using integration by parts, that if v' satisfies (2.1'), then

$$\langle v_\alpha, Lv'\rangle = -\lambda_\alpha\langle v_\alpha, v'\rangle - [v_\alpha(\kappa Q/(f_0 H\bar{u}) - N^2 f_0^{-1}\partial_x h)]_{z=0}. \quad (2.6)$$

Multiplying (2.2) by $\rho_0 v_\alpha \bar{u}^{-1}$, integrating over z, and using (2.6) one obtains the horizontal structure equation,

$$(\nabla^2 - \lambda_\alpha)\langle v', v_\alpha\rangle = -f_0 H^{-1} v_\alpha(0)\partial_x h - \kappa f_0 H^{-1}\langle QN^{-2}\partial_z(v_\alpha \bar{u}^{-1})\rangle. \quad (2.7)$$

Once (2.7) has been solved, v' can be determined from

$$v'(x, y, z) = \sum_\alpha \langle v', v_\alpha\rangle(x, y)v_\alpha(z), \quad (2.8)$$

where the summation represents a sum over the discrete spectrum and integration over the continuum. This is an inconvenient way of expressing the solution immediately above orography, for the v_α satisfy homogeneous boundary conditions, and as a result the convergence of the series (2.8) to the solution is nonuniform. We are primarily concerned here with the remote response to localized forcing for which, on the contrary, this is a particularly convenient way of expressing the solution.

Using (2.5a) one can rewrite the thermal forcing on the right-hand side of (2.7) as

$$\kappa H^{-1}\langle w_\alpha Q\bar{u}^{-2}\rangle. \quad (2.9)$$

The latter form makes it clear that heating confined to the immediate vicinity of the surface is inefficient at forcing a stationary response, since $w_\alpha(0) = 0$. However, the factor $\bar{u}^{-2}$ mitigates this effect to a great extent when surface winds are small.

If $\lambda_\alpha > 0$, the mode α is horizontally trapped in the vicinity of a localized source. If $\lambda_\alpha < 0$, the mode is horizontally wavelike with total horizontal wavenumber $K_\alpha^2 = (-\lambda_\alpha)^{1/2}$, and (2.7) must be solved with the appropriate radiation conditions. That discrete mode with the smallest (most negative) λ_α is called the external mode and denoted by the subscript e. We assume that $\lambda_e < 0$ for the remainder of this section, a restriction justified in Sections 3–5.

Suppose that the heating and topography are localized. Then as one moves horizontally away from the source at fixed height, the horizontally wavelike modes become dominant in (2.8). Furthermore, the

contribution from the horizontally wavelike continuum modes decays algebraically downstream, due to destructive interference, leaving the horizontally wavelike discrete modes to dominate the response. It is therefore of great importance for the structure of the stationary wave field that there is generally only a single discrete mode v_e trapped within the troposphere, which then comes to dominate the tropospheric solution at some distance from the source. (As will be shown in Section 2c, this distance can be quite short.) Layered models with rigid-lid upper boundary conditions inevitably introduce artificial discrete modes. The ability of such models to simulate the tropospheric stationary wave field far from the source is dependent on whether these artificial discrete modes are horizontally wavelike or evanescent. This question is discussed in Section 5.

For a discrete mode, $\rho_0 w_\alpha \to 0$ as $z \to \infty$, so that $K_\alpha^2 = -\lambda_\alpha = \beta\langle v_\alpha\rangle/\langle \bar{u} v_\alpha\rangle$ from (2.5b). If one defines an equivalent barotropic wind $u_e \equiv \beta/K_e^2$ for the external mode, then

$$u_e = \langle \bar{u} v_e\rangle/\langle v_e\rangle. \tag{2.10}$$

The equivalent barotropic level z_e is then defined so that $\bar{u}(z_e) = u_e$. This is the conventional definition; from (2.5b), $\partial_z(\rho_0 w_e) = 0$ at this level. Equation (2.7) implies that the contribution of the external mode to v' at the equivalent barotropic level, $V \equiv \langle v' v_e\rangle v_e(z_e)$, is the solution to

$$(\nabla^2 + \beta u_e^{-1})V = -f_0 H^{-1}\partial_x h_e \tag{2.11}$$

where

$$\partial_x h_e \equiv v_e(0)v_e(z_e)\partial_x h + \kappa v_e(z_e)\langle QN^{-2}\partial_z(v_e\bar{u}^{-1})\rangle. \tag{2.12}$$

The familiar stationary response V_B to flow over topography h_B in a quasi-geostrophic shallow-water model, linearized about the constant zonal flow $\bar{u}$, is given by

$$(\bar{u}\nabla^2 + \beta)V_B = -\bar{u} f_0 H_B^{-1}\partial_x h_B, \tag{2.13}$$

where H_B is the mean depth. Thus, in regions where the external mode dominates, the barotropic model (2.13) is correct provided 1) that it is applied at the equivalent barotropic level z_e, and 2) that h_B/H_B is set equal to h_e/H, where H is the scale height and h_e the equivalent topography defined by (2.12).

The factor multiplying the true topography for use in such a barotropic model is

$$\alpha \equiv v_e(0)v_e(z_e), \tag{2.14}$$

assuming that $H_B = H$. From the boundary condition in (2.3), one knows that $v_e(0) \to 0$, and therefore $\alpha \to 0$, as $\bar{u}(0) \to 0$. Since $\bar{u}(0)$ is typically small, it is more convenient to define

$$\alpha_s \equiv v_e(0)v_e(z_e)u_e/\bar{u}(0). \tag{2.15}$$

The right-hand side of the equivalent barotropic model (2.13) then reads

$$-\alpha_s f_0 \bar{u}(0)H^{-1}\partial_x h. \tag{2.16}$$

The replacement of u with $\bar{u}(0)$ on the right-hand side of (2.13) while retaining $\bar{u} = u_e$ on the left-hand side is often motivated (e.g., Hoskins and Pearce, 1983, their Appendix A.3) by assuming that the perturbation is separable $v' = A(z)B(x, y)$, substituting into the vorticity equation in (2.1), vertically integrating, and then using the lower boundary condition $w' = \bar{u}(0)\partial_x h$. If one sets $A = v_e$, the result at $z = z_e$ is

$$(u_e\nabla^2 + \beta)v' = -f_0\bar{u}(0)v_e(z_e)\partial_x h/(\langle v_e\rangle H).$$

This does not reduce to the correct topographic forcing given by (2.12) or (2.16), since

$$v_e(z_e)\bar{u}(0)/(u_e\langle v_e\rangle) = v_e(z_e)\bar{u}(0)/\langle uv_e\rangle \neq \alpha. \tag{2.17}$$

The error arises because the forced wave has nonzero projection onto more than one mode and, therefore, is not separable. It is only far from the source and within the troposphere that the solution is approximately separable, when it is dominated there by the external mode.

c. *An example of vertical modal decomposition*

As a simple example of vertical modal decomposition, we choose $\bar{u}$ and N^2 independent of z and solve for the Green's function in the (x, z) plane for topography that varies sinusoidally in y, that is, the stationary response to the topography $h = A\delta(x) \times \sin(ly)$, where A has units of (length)^2. We set $v' = AN\sin(ly)e^{z/2H}\partial_x\eta$, and then nondimensionalize horizontal distances by L, vertical distances by H, and velocities by βL^2, where $L \equiv NH/f_0$, using the same symbols for the nondimensional variables. The problem to be solved becomes

$$\partial_{zz}\eta + \partial_{xx}\eta - V_0\eta = 0, \quad z \geq 0;$$
$$\partial_z\eta + \eta/2 = -\delta(x), \quad z = 0. \tag{2.18}$$

with $V_0 \equiv 1/4 + l^2 - \bar{u}^{-1}$.

The vertical eigenvalue problem is

$$\partial_{zz}\eta = (V_0 - \lambda)\eta, \quad z \geq 0;$$
$$\partial_z\eta + \eta/2 = 0, \quad z = 0. \tag{2.19}$$

Assume for definiteness that $V_0 < 0$. The discrete spectrum consists of the mode $\eta_e = e^{-z/2}$, for which $\lambda_e = V_0 - 1/4$, or $k_e^2 = \bar{u}^{-1} - l^2$. As is well known, the geopotential perturbation in this simplest external Rossby wave is independent of height. The eigenfunctions of the continuous spectrum are $\eta_n = (2/\pi)^{1/2}\cos(nz_n + \varphi_n)$, for which $\lambda_n = V_0 + n^2$ and $\tan(\varphi_n) = (2n)^{-1}$. The eigenfunctions have been normalized so that (2.4) is satisfied; in particular,

$$\int_0^\infty \eta_n\eta_{n'}dz = \delta(n - n').$$

The solution for the Green's function is

$$\eta = \chi_e(x)\eta_e(z) + \int_0^\infty \chi_n(x)\eta_n(z)dn, \quad (2.20)$$

where

$$(\partial_{xx} + k_e^2)\chi_e = -\delta(x),$$

$$(\partial_{xx} - V_0 - n^2)\chi_n = -\eta_n(0)\delta(x).$$

Since the zonal group velocity of stationary Rossby waves is positive (for nonzero zonal wavenumber), one has for the external mode

$$\chi_e = \begin{cases} -k_e^{-1}\sin(k_e x), & x > 0 \\ 0, & x < 0; \end{cases} \quad (2.21a)$$

and for the continuum,

if $\mu \equiv |V_0| - n^2 > 0$:

$$\chi_n = \begin{cases} -\eta_n(0)\mu^{-1/2}\sin(\mu^{1/2}x), & x > 0 \\ 0, & x < 0; \end{cases} \quad (2.21b)$$

if $\nu \equiv n^2 - |V_0| > 0$:

$$\chi_n = \eta_n(0)\nu^{-1/2}\exp(-\nu^{1/2}|x|). \quad (2.21c)$$

Thus, one can divide η into three parts, $\eta = \eta_1 + \eta_2 + \eta_3$, where $\eta_1 = \chi_e(x)\eta_e(z)$ is the contribution from the vertically trapped, horizontally propagating external mode, η_2 [that part of the integral in (2.20) from $n = 0$ to $n = |V_0|^{1/2}$] is the contribution from the vertically and horizontally propagating modes, and η_3 (the integral from $|V_0|^{1/2}$ to ∞) is the contribution from the vertically propagating but horizontally trapped modes. If $x < 0$, only η_3 contributes. Since $\eta_2 + \eta_3 = O[(x^2 + z^2)^{-1/2}]$ for $x > 0$, η_1 dominates near the ground as $x \to \infty$.

More conventionally, one solves (2.18) by Fourier transforming in x and applying a radiation condition as $z \to \infty$ for each Fourier component. The result is

$$\eta = (2\pi)^{-1}\int_C dk(m - 1/2)^{-1}e^{i(kx-mz)} + (\text{c.c}), \quad (2.22)$$

where $m \equiv (k^2 - |V_0|)^{1/2}$ and where C runs from the origin to $+\infty$ along the real k-axis, following the lower lip of the square root branch cut, as shown in Fig. 1. Also, C must pass under the pole at $m = 1/2$, or $k = k_e$, since this pole moves into the upper half-plane if one adds damping or solves an initial value problem.

The equivalence of the vertical modal (2.20–2.21) and the zonal modal decompositions can be seen by deforming the contour C in (2.22). If $x < 0$, one can close in the lower half-plane, as shown in Fig. 1, and the integration over C can be replaced by integration along the imaginary k-axis. If $x > 0$, integration over C can be replaced by contributions from 1) the pole, 2) the integrations along both sides of the branch cut and 3) integration along the imaginary axis. Straightforward manipulation shows that the contribution from the pole equals the external mode solution η_1, the integration along both sides of the branch cut equals η_2, and the integrations along the imaginary k-axis equal η_3.

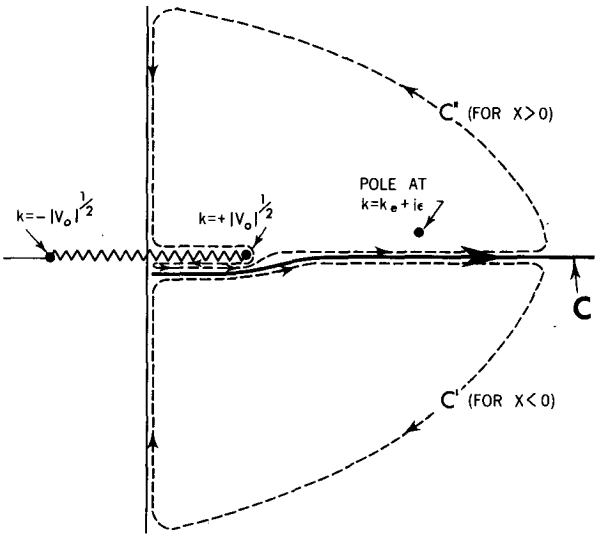

FIG. 1. The contour C in the complex k-plane used in evaluating (2.22). The integral around the dashed contour C' equals zero, and if $x < 0$ the integral over C can therefore be replaced by an integral along the imaginary k-axis. The integral around C'' equals the residue at the external mode pole; therefore for $x > 0$ the integral over C can be replaced by this residue plus the contribution from integrating around the branch cut, plus an integral along the imaginary k-axis.

Figure 2 is a plot of the geopotential, $\Phi(x, z) = e^{z/2}\eta$ for the case $k_e = 0.7$, $l = 0$. Since the external mode's contribution to Φ is independent of z in this simple special case, it is clear from Fig. 2 where it dominates the response. Figure 3 compares the total perturbation geopotential at $z = 0$ with the external mode contribution. This figure emphasizes that despite the gross discrepancy near the source, where $\Phi(x, 0) \approx -\ln(x)/\pi$, the first downstream trough is still very well captured by the external mode in isolation. The qualitative behavior of the Green's function in Fig. 2, with the external mode contribution dominant in the troposphere except in the immediate vicinity of the source, is also seen in stationary wave Green's functions for more realistic basic state winds (e.g., Held, 1983). The most noteworthy difference is that if $\bar{u}$ has vertical structure, then the external mode does also.

d. Vertical structure of the external mode

For arbitrary $N^2(z)$, $\bar{u}(z) > 0$, the standard transformation $\eta \equiv b^{1/2}v_\alpha$, with $b \equiv \rho_0 N^{-2}$, converts (2.3) into

$$\partial_{zz}\eta + (N^2 f_0^{-2}\bar{u}^{-1}\bar{q}_y - b^{-1/2}\partial_{zz}b^{1/2})\eta = -N^2 f_0^{-2}\lambda\eta \quad (2.23)$$

with the boundary condition

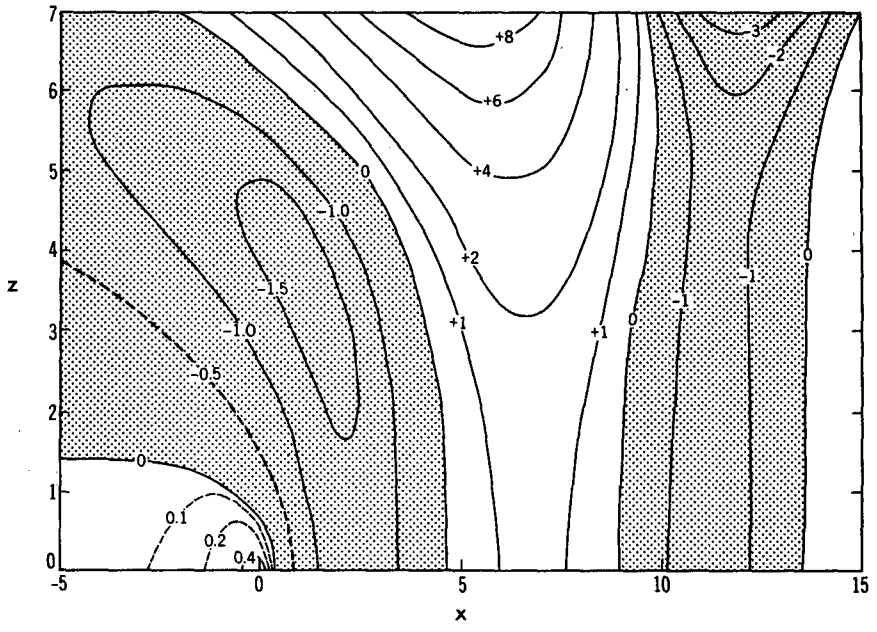

FIG. 2. Linear stationary geopotential height response to the mountain $h = A\delta(x)$, assuming that $\bar{u}$ and N^2 are constant. Horizontal distance is nondimensionalized by NH/f and vertical distance by H, the scale height. In these units, the stationary wavenumber is 0.7. The dimensional geopotential is obtained by multiplying by AN/f_0. Shaded areas are negative.

$$\partial_z\eta = \eta[\bar{u}^{-1}\partial_z\bar{u} + (2b)^{-1}\partial_z b], \quad z = 0. \quad (2.23')$$

As in Bretherton (1966), the boundary condition can be satisfied by adding a δ-function to the potential. The resulting equation is

$$(-\partial_{zz} + V)\eta = N^2 f_0^{-2}\lambda\eta, \quad -\infty < z < \infty, \quad (2.24)$$

where

$$V(z) = V(-z) \equiv -N^2 f_0^{-2}\bar{u}^{-1}\bar{q}_y + b^{-1/2}\partial_{zz}b^{1/2} + 2[\bar{u}^{-1}\partial_z\bar{u} + (2b)^{-1}\partial_z b]\delta(z). \quad (2.25)$$

Solutions of (2.24) that are symmetric about $z = 0$ are also solutions of (2.23). The external mode is the

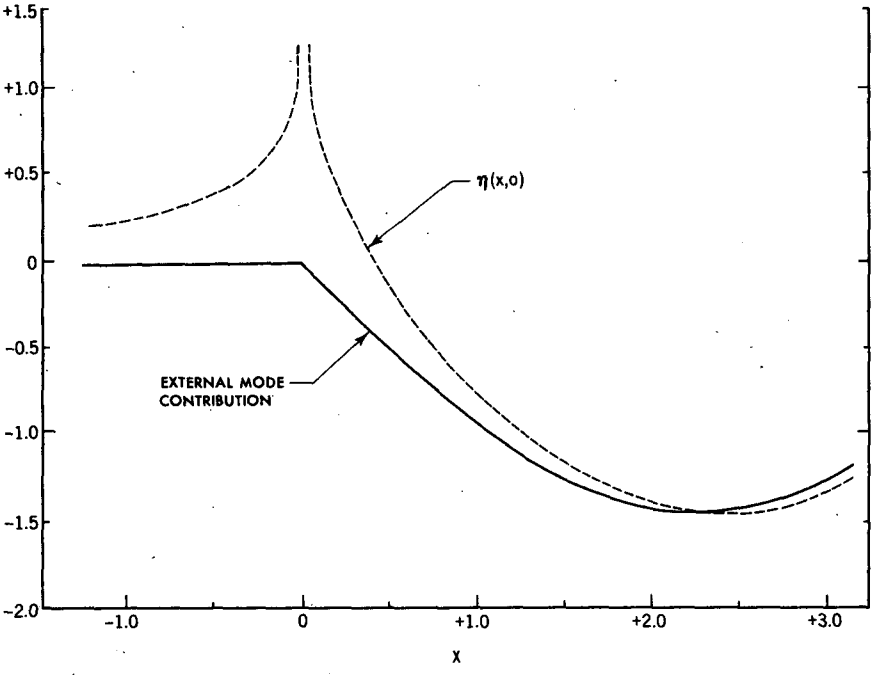

FIG. 3. Comparison of the full baroclinic Green's function shown in Fig. 2 evaluated at the surface, and the contribution of the external mode given by (2.21a).

lowest bound state of the potential V. If $V \to V(\infty)$ and $N \to N(\infty)$ as $z \to \infty$, then all discrete modes satisfy $\tilde{\lambda} < V(\infty)$, while the continuous spectrum is characterized by $\tilde{\lambda} > V(\infty)$, where $\tilde{\lambda} \equiv N^2(\infty) f_0^{-2} \lambda$. If $V(\infty) < 0$, then the continuous spectrum consists of horizontally propagating as well as horizontally trapped modes.

For constant $\bar{u}$ and N^2, the potential is constant except for an attractive δ-function at the origin. Such a potential has the one bound state discussed above, $\eta_e = e^{-z/2H}$ or $v_e = 1$, with $K_e^2 = \beta/\bar{u}$. In this special case, the vertical velocity and the thermal forcing of the mode are identically zero [see (2.7)]. For the linear shear profile $\bar{u} = u_0 + \Lambda z$, with typical midlatitude values for Λ and u_0, the external mode has the structure shown in Fig. 4 (see Section 3 for detailed discussion). As expected for the lowest bound state, v_e is of the same sign for all z. The corresponding eigenvalue λ_e is negative, so the mode is horizontally wavelike. The surface δ-function is now repulsive, since $\bar{u}^{-1}\partial_z \bar{u}$ is much greater than $-(2b)^{-1}\partial_z b = (2H)^{-1}$ at the surface, and the mode is trapped instead in a potential well created by the increasing westerlies. Despite this fundamental difference, the external mode in Fig. 4 evolves continuously from the simple external mode $v_e = 1$ as the vertical shear is increased from zero.

Because of the repulsive δ-function, η_e increases away from the surface and, therefore, v_e (or the geopotential) increases faster than $e^{z/2H}$. More precisely, the lower boundary condition implies that $\partial_z(v_e/\bar{u}) = 0$ at $z = 0$; therefore, the increase in v_e with height near the ground is similar to that of $\bar{u}$. Maximum amplitude in η_e occurs considerably below the mode's turning point in the potential well, which occurs near $z = 2H$ for the parameters chosen for the figure; maximum geopotential amplitude occurs somewhat higher and closer to the turning point. The cold lows and warm highs below the geopotential maxima serve to distinguish these remotely forced waves from the cold highs and warm lows typically forced by local heating.

The sign of the vertical motion in the external mode is easily obtained from the vorticity equation (2.5b). The term $\partial_z(\rho_0 w_e)$ has the same sign as $(\beta K_e^{-2} - \bar{u})v_e$; therefore, for monotonically increasing $\bar{u}(z)$, $\partial_z(\rho_0 w_e)$ is of the same sign as v_e below the equivalent barotropic level z_e, and opposite in sign to v_e above z_e, implying that w_e and v_e are in phase for all z. We find that this result remains valid over most of the fluid for more realistic basic states. Since the thermodynamic equation (2.5a) can be written $\partial_z(v_e/\bar{u}) = -N^2 f_0^{-2}\bar{u}^{-2} w_e$, we have the result that $\partial_z(v_e/\bar{u})$ is opposite in sign to v_e. Therefore, v_e increases with height but less rapidly than $\bar{u}$. Equation (2.12) then implies that positive perturbation heating is equivalent to a negative topographic slope insofar as the far field is concerned.

The meridional displacement of streamlines in the presence of a steady wave is $\xi' = -\psi'(\partial_y \bar{\Psi})^{-1} = \psi'/\bar{u}$. The preceeding discussion implies that the displacements $\xi_e(z)$ created by the external mode have maximum amplitude at the ground. The same will be true of the perturbation potential vorticity, $q_e = -\xi_e \bar{q}_y$, as long as $\bar{q}_y$ has little vertical structure. The eddy vorticity and potential vorticity are in phase, $q_e = \zeta_e u_e \bar{q}_y/(\bar{u}\beta)$, but q_e generally decreases away from the surface while $\zeta_e = -K_e^2 \psi_e$ increases. The vertical structures of w_e, $q_e \propto v_e/\bar{u}$, $T_e \propto \partial_z \psi_e$, and $Q_{\text{EFF}} = -\partial_z(v_e/\bar{u})$ for the linear shear profile, illustrated in Fig. 4, are consistent with these arguments. The structure in Q_{EFF} at low levels implies that the far field response is very sensitive to the vertical structure of the heating when the heating is confined near the surface.

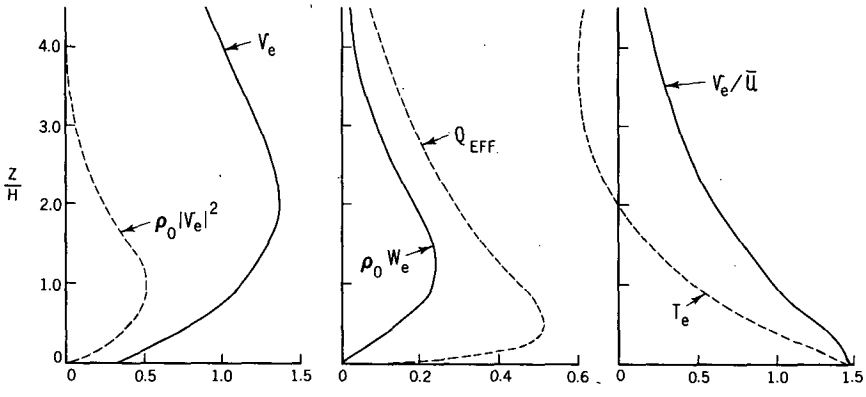

FIG. 4. Vertical structure of the external mode on the flow $u = u_0 + \Lambda z$, with $u_0 = 0.2(\Lambda H)$ and $r = \beta N^2 H/(f^2 \Lambda) = 1.0$. Plotted are v_e, the geopotential (or meridional velocity) amplitude normalized according to (2.4); $\rho_0|v_e|^2$; $\rho_0 w_e$, the density weighted vertical velocity; $Q_{\text{EFF}} = -\partial_z(v_e/\bar{u})$, the heating efficiency factor appearing in (2.7); the temperature structure T_e (or, equivalently, $\partial_z v_e$); and the amplitude of the meridional particle displacement $v_e/\bar{u}$ (also proportional to the potential vorticity perturbation).

e. Group velocity and damping

In designing an equivalent barotropic model for stationary waves, one should try to include damping that mimics the effects on external Rossby waves of various dissipative mechanisms of importance in the atmosphere. We address this problem briefly here and in more detail in a forthcoming paper (Held *et al.*, 1985). Consider a plane wave external mode solution to the homogeneous version of (2.1′)–(2.2) [$\psi' \doteq \psi_e(z)\exp(ikx + ily)$, $\psi_e \propto v_e$, $k^2 + l^2 = K_e^2$] and perturb this wave by adding small height-independent linear damping of eddy vorticity, $-\gamma\zeta'$, and of temperature, $-\gamma\partial_z\psi'$. If we set $\bar{u}(z) = u_0 + f(z)$, the introduction of damping has the effect of replacing u_0 with $u_0 - i\gamma k^{-1}$, or K_e^2 with $K_e^2 - i\gamma k^{-1}\partial K_e^2/\partial u_0$, where the partial derivative is taken with fixed $f(z)$. Since the unperturbed wave satisfies $(\nabla^2 + K_e^2)\partial_x\psi' = 0$, the weakly damped stationary external wave satisfies the horizontal structure equation

$$(\nabla^2 + K_e^2)\partial_x\psi' = -\gamma(\partial K_e^2/\partial u_0)\psi' = \gamma K_e^{-2}(\partial K_e^2/\partial u_0)\zeta'. \quad (2.26)$$

Therefore, the vorticity equation, $u_e\partial_x\zeta' + \beta v' = -\gamma_e\zeta'$, predicts the correct spatial decay provided that

$$\gamma_e = \gamma u_e K_e^{-2}(-\partial K_e^2/\partial u_0) \equiv \gamma g. \quad (2.27)$$

If the problem were Galilean invariant, one could make the correspondence $u_0 \to -c$ and relate γ_e to the group velocity of the external mode. For transient waves, the term $\partial_t(\partial_z\psi' - N^2g^{-1}\psi')$ must be added to the left-hand side of (2.1′) [g here refers to the acceleration of gravity, not to the quantity defined in (2.27)]. The term $N^2g^{-1}\psi'$ prevents exact invariance, but is extremely small ($\approx 0.02\partial_z\psi'$) for quasi-stationary external waves in realistic vertical shears. We therefore ignore this correction and replace u_0 with $-c$ in (2.27). Since the group velocity of a wave with phase speed $c(K^2)$, evaluated in a frame of reference in which $c = 0$, is

$$\mathbf{G} = (G_x, G_y) = k\nabla_k c = 2k\mathbf{k}\partial c/\partial K^2$$

where $\mathbf{k} \equiv (k, l)$, we have

$$\mathbf{G}_e = -2k\mathbf{k}(\partial K_e^2/\partial u_0)^{-1} \quad (2.28)$$

for the external mode. The correction factor g in (2.27) is seen to be the ratio of the group velocity of a Rossby wave in that equivalent barotropic model with the correct stationary wavenumber,

$$\mathbf{G}_B = 2\beta k K_e^{-4}\mathbf{k} = 2u_e k K_e^{-2}\mathbf{k},$$

to the true group velocity of the external mode. As discussed in Sections 3–5, g is typically less than unity.

The following expression relating $\partial K_e^2/\partial u_0$ or g to the vertical structure of the mode is derived in the Appendix:

$$g = u_e\{\langle v_e^2\bar{u}^{-1}\rangle + f^2K_e^{-2}\langle N^{-2}(\partial_z v_e)\partial_z(v_e/\bar{u})\rangle\}. \quad (2.29)$$

The first term in angle brackets is always positive, while the second is generally negative since, as argued in Section 2*d*, $\partial_z(v_e/\bar{u})$ is typically opposite in sign to v_e and, therefore, to $\partial_z v_e$. However, in nearly all cases the sum is positive, so that $\mathbf{G}_e$ is in the same direction as $\mathbf{G}_B$. The only exception we have found is in the two-layer model when surface winds are small and the shear is supercritical (Panetta *et al.*, 1985).

If the inviscid wave is modified by adding a small amount of Ekman pumping, the lower boundary condition becomes

$$\bar{u}\partial_z v' - v'\partial_z\bar{u} = -HN^2f^{-2}\gamma_{\rm Ek}\nabla^2\psi', \quad z = 0. \quad (2.30)$$

$\gamma_{\rm Ek}^{-1}$ is the Ekman spindown time in the purely barotropic special case (u and ψ' independent of z). A calculation analogous to that leading to (2.29) results in

$$\gamma_e = \gamma_{\rm Ek}u_e v_e(0)^2\bar{u}(0)^{-1} \equiv \gamma_{\rm Ek}g_{\rm Ek}. \quad (2.31)$$

Ekman pumping is inefficient if $u(0)$ is small, since $g_{\rm Ek}$ is proportional to

$$v_e^2\bar{u}^{-1}|_{z=0} = v_e\partial_z v_e(\partial_z\bar{u})^{-1}|_{z=0} \quad (2.32)$$

and $v_e(0) \to 0$ as $\bar{u}(0) \to 0$.

3. External modes in a linear shear flow

Following Charney (1947), it is illuminating to consider in detail the flow $\bar{u}(z) = u_0 + \Lambda z$ on a beta-plane, with u_0 and Λ positive constants, and with uniform N^2. For such a flow $\bar{q}_y = \beta(1 + r^{-1})$, where $r \equiv \beta N^2H/(f^2\Lambda)$. Defining $\eta = \psi' e^{-z/2H}$, and then nondimensionalizing using H, NH/f, and $H\Lambda$ for the vertical length, horizontal length, and horizontal velocity scales, the eigenvalue problem for stationary waves is reduced to the form $-\partial_{zz}\eta + V\eta = \lambda\eta$, $-\infty < z < \infty$, with

$$V(z) = 1/4 - (1 + r)(u_0 + z)^{-1} + (2u_0^{-1} - 1)\delta(z). \quad (3.1)$$

The remaining nondimensional parameters in the problem are u_0 and r. For typical midlatitude conditions, $r \approx 1$ while $u_0 \lesssim 0.3$.

Since $V(\infty) - V(z) = O(z^{-1})$ for large z, the discrete spectrum consists of a countably infinite set with an accumulation point at $\lambda = V(\infty) = 1/4$. The infinite number of modes is due to the fact that the turning point $z_T = (1 + r)(1/4 - \lambda)^{-1} - u_0$, at which $V(z) = \lambda$, recedes to $+\infty$ as $\lambda \to 1/4$ in such a way that the WKB phase integral

$$\int^{z_T}(V - \lambda)^{1/2}dz \quad (3.2)$$

also becomes infinite. Hence, there are infinitely many values of λ near 1/4 for which η has the proper

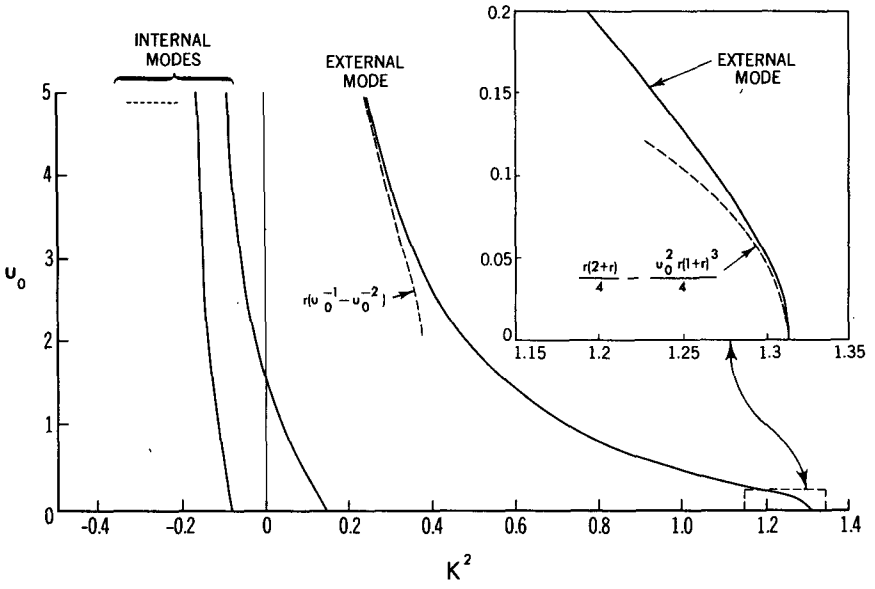

FIG. 5. The nondimensional squared horizontal wavenumber $K^2 = -\lambda$, as a function of nondimensional surface wind u_0, for the discrete modes in Charney's model with $r = 1.5$. The insert emphasizes the fact that $\partial K_e^2/\partial u_0 \to 0$ as $u_0 \to 0$.

phase to match to an exponentially decaying solution above the turning point. The continuous spectrum extends from $\lambda = 1/4$ to ∞ and consists of vertically propagating, horizontally trapped modes only, since $V(\infty) > 0$.

Burger's (1962) analysis of Charney's model provides essential information on the neutral modes of interest here. Recasting Burger's results in our notation, he finds for the discrete spectrum that

$$\lambda_n \to 1/4 - [(1 + r)/2n]^2 \qquad (3.3)$$

as u_0 approaches 0, where n is a positive integer. It follows that for sufficiently small u_0, the number of horizontally wavelike discrete modes (those with $\lambda < 0$) equals the largest integer less than $1 + r$. The corresponding eigenfunction for the external mode ($n = 1$) approaches $v_e \propto ze^{-rz/2}$ as $u_0 \to 0$. In this limit, v_e reaches its maximum value at $z = 2/r$, the temperature perturbation decreases away from the surface, $\partial_z v_e \propto (1 - rz/2)e^{-rz/2}$, the meridional displacements (or, equivalently, the potential vorticity perturbations) have maximum amplitude at the surface, $v_e/u \propto e^{-rz/2}$, while $\rho_0 w_e$ is proportional to $z^2 \exp[-(1 + r/2)z]$.

Explicit calculation shows that λ_n increases as u_0 increases, for each n. For the wavelike modes this implies that the horizontal wavenumber $K_e = (-\lambda_e)^{1/2}$ decreases with increasing westward phase speed of the wave with respect to the mean winds, as expected for Rossby waves. Specifically, as u_0 increases from 0 to ∞, the external mode eigenvalue, $\lambda_e = \lambda_1$, increases monotonically from $-r(2 + r)/4$ [see (3.3)] to 0. Therefore, *the external mode is always horizontally wavelike.* In contrast, for all $n > 1$, $\lambda_n \to 1/4$ as $u_0 \to \infty$, implying horizontal evanescence for sufficiently large u_0. The plot in Fig. 5 of the first three eigenvalues as a function of u_0, for $r = 1.5$, illustrates this behavior. The curves were obtained using series expansions for the eigenfunctions, as outlined in Pedlosky (1979), and iterating to find the eigenvalues.

It follows from the foregoing that if $r < 1$, there is one and only one vertically trapped, horizontally wavelike mode—the external mode; for $1 < r < 2$, there must be two such modes for sufficiently small u_0, but only one for sufficiently large u_0, etc. Figure 6 shows a computation of the number of horizontally wavelike modes given $0 < r < 4$, $0 < u_0 < 2.0$.

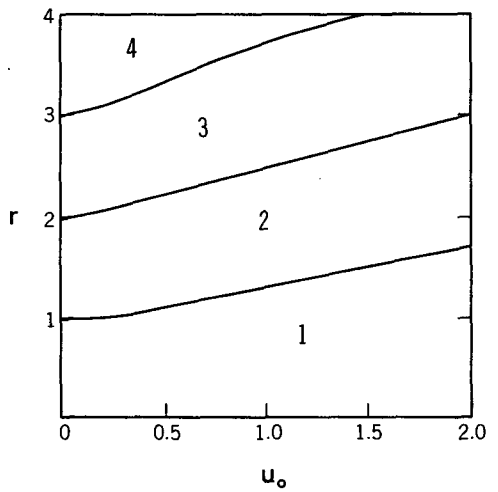

FIG. 6. Number of horizontally propagating stationary modes in Charney's model as a function of r and u_0.

It is useful to have expressions for the external mode stationary wavenumber $K_e = (-\lambda_e)^{1/2}$ in the two limits $u_0 \ll 1$ and $u_0 \gg 1$. The former limit is of relevance to the extratropical troposphere, while the latter limit makes the connection with the familiar case of constant u. Using standard perturbation theory one can show for large u_0 that

$$K_e^2 \approx r u_0^{-1}(1 - u_0^{-1}), \tag{3.4}$$

or $K_e^2 \approx \beta u_0^{-1}(1 - \Lambda H u_0^{-1})$ dimensionally, as plotted in Fig. 5. Defining the equivalent barotropic height as before, we have $K_e^2 = r/(u_0 + z_e)$. Comparison with (3.4) shows that $z_e \to 1$ as $u_0 \to \infty$ (i.e., as the vertical shear approaches zero, for fixed surface wind).

As surface winds approach zero, $K_e^2 \to r/z_e$, by definition of z_e. But we know from (3.3) that $K_e^2 \to r(2 + r)/4$ as $u_0 \to 0$. Therefore,

$$z_e \to 4/(2 + r) \quad \text{as} \quad u_0 \to 0. \tag{3.5}$$

In this limit, the dimensional equivalent barotropic height is greater than one scale height as long as $r < 2$, and is bounded above by $2H$. This result seems to justify the common choice of upper tropospheric zonal mean winds for use in linear barotropic models. (However, Charney's model overestimates this height somewhat, as discussed in Sections 4 and 5.) Using the explicit solutions to Charney's model, one can show that

$$K_e^2 = r(2 + r)/4 - u_0^2 r(1 + r)^3/4 + O(u_0^3) \tag{3.6}$$

(see Fig. 5), from which one finds that

$$z_e = 4/(2 + r) - u_0 + 4(1 + r)^3(2 + r)^{-2}u_0^2 + O(u_0^3). \tag{3.7}$$

Plots of z_e as a function of u_0 for several values of r are included in Fig. 7. While not necessarily monotonic, $z_e(u_0)$ evidently has little structure between its two limiting values, $z_e(0) = 4/(2 + r)$ and $z_e(\infty) = 1$.

Given the vertical structure of the external mode, one can compute the appropriate topographic stretching for use in an equivalent barotropic model, $\alpha u_e f_0 H^{-1}\partial_x h = \alpha_s \bar{u}(0) f_0 H^{-1}\partial_x h$, where α and α_s are defined by (2.14) and (2.15). One can think of α (or α_s) as a correction to be used when computing the stretching by blowing the equivalent barotropic wind (or surface wind) over the topography. The α and α_s are plotted in Fig. 7 as functions of u_0 for several values of r. Typically, α is smaller than unity, and α_s larger than unity; both approach unity as $u_0 \to \infty$; α is proportional to u_0, and α_s approaches a constant, $S(r)$, as $u_0 \to 0$. The normalized eigenfunction sufficiently accurate for small u_0 to compute $S(r)$ turns out to be

$$v_e = \delta^{1/2}[2\delta(u_0 + z)]e^{-rz/2}; \quad \delta \equiv (1 + r)/2. \tag{3.8}$$

Therefore,

$$S(r) = 8(1 + r)^3(2 + r)^{-2}e^{-2r/(2+r)}, \tag{3.9}$$

so that S varies monotonically from 2.0 at $r = 0$ to 4.9 at $r = 2$. As indicated in Fig. 7, α_s varies significantly as u_0 and r vary when u_0 is small.

Figure 7 also shows the ratio g of the barotropic to correct baroclinic group velocity as obtained from (2.27), once again as a function of u_0 for several values of r. As $u_0 \to \infty$, the two group velocities approach one another. However, for small u_0, the barotropic model seriously underestimates the group velocity. Indeed, from (3.6) the dimensional group velocity for a zonally directed ray approaches

$$\Lambda H u_0^{-1}(2 + r)(1 + r)^{-3} \tag{3.10}$$

as $u_0 \to 0$. This infinite group velocity is replaced with a very large value when the non-Doppler term in the lower boundary condition is retained (see Section 2e.) More pertinently, it disappears when $\bar{u}(z)$ is modified so that winds do not increase indefinitely with height, as described in Section 4.

According to (2.27), g is also the factor to be multiplied into the damping rate γ, to convert it into the rate appropriate for use in a barotropic model, if thermal and mechanical damping rates are equal and independent of height. Also plotted in Fig. 7 is the analogous correction factor for Ekman pumping, g_{Ek}, defined by (2.31). It is easily verified from (3.8) that $g_{Ek} \to 2u_0(1 + r)^3/(2 + r)$ as $u_0 \to 0$. Thus, both g and g_{Ek} approach zero as $u_0 \to 0$, but for different reasons: g vanishes because the group velocity becomes infinite in this limit, while g_{Ek} vanishes because the amplitude of the external mode at the surface vanishes. For more complex basic states, g_{Ek} still vanishes in this limit while g does not. We emphasize that other combinations of thermal and mechanical damping can lead to very different results.

4. Vertical modes for more realistic wind and static stability profiles

Charney's model emphasizes the importance of the shear parameter r in determining the characteristics of the discrete modes; in particular, $r > 1$ is required for the existence of more than one horizontally wavelike mode. In the present section we relax the unrealistic assumption of uniform wind shear and also investigate the effects of a tropopause. The delineation of the circumstances under which more than one horizontally wavelike discrete mode can exist will be of particular interest. We are also concerned with the extent to which Charney's model distorts the amplitude of topographically forced external waves and the group velocity of these stationary waves.

Throughout this discussion we will make use of nondimensional variables with unit of depth H, unit of length $N(0)H/f$, and unit of velocity $\bar{u}_z(0)H$. In these units, the shear at the ground equals one. We also define $r_0 = \beta N^2(0)H/[f_0^2 \bar{u}_z(0)]$, the nondimensional Charney parameter based on ground level

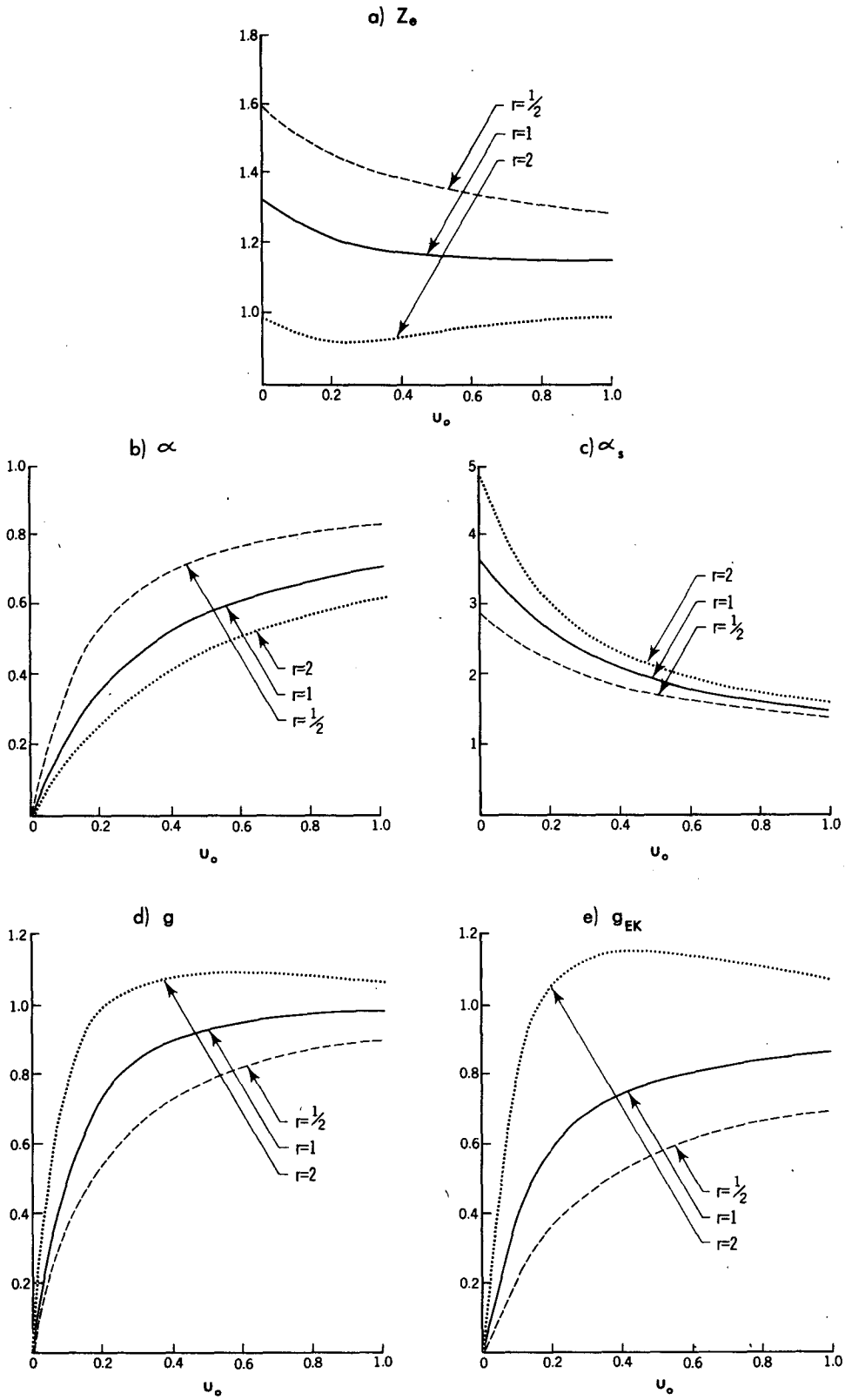

FIG. 7. Parameters needed in designing an equivalent barotropic model, as a function of u_0, for three values of r: (a) equivalent barotropic height divided by the scale height; (b) and (c) correction factors to be multiplied into u_e and u_0, respectively, before computing vortex tube stretching (see Sec. 2); (d) ratio of group velocity of stationary mode in barotropic model to that of the external mode; (e) factor to be multiplied into barotropic Ekman damping rate.

TABLE 1. The nondimensional total horizontal wavenumber K_e, equivalent barotropic height z_e, surface wind amplification factor α_s, and group velocity ratio g, for the stationary external Rossby wave on the four wind profiles (4.1a–d), assuming that $u_0 = 0.2141$, $z_w = 1.5$, $z_T = 1.5$, $z_J = 0.5$, and $r_0 = 0.5$. Results are shown both with constant N^2 and with a tropopause ($N_s^2 = 2.5N_T^2$). The asterisk signifies that a second mode exists; two asterisks indicate a metastable state.

	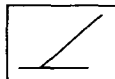		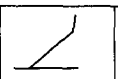		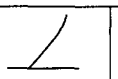		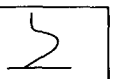	
$(N_s/N_t)^2$	1	2.5	1	2.5	1	2.5	1	2.5
K_e	0.55	0.58*	0.64	0.64	0.68	0.69	0.77**	0.77**
Z_e	1.46	1.29	1.01	0.99	0.98	0.94	0.68	0.68
α_s	2.21	2.30	1.58	1.67	1.53	1.67	1.22	1.22
g	0.58	0.68	0.74	0.75	0.79	0.81	—	—

shear and static stability. The following four velocity profiles will be considered:

$$\bar{u} - u_0 = z, \tag{4.1a}$$

$$\bar{u} - u_0 = \begin{cases} z, & z < z_w \\ z_w, & z \geqslant z_w, \end{cases} \tag{4.1b}$$

$$\bar{u} - u_0 = z_w \tanh(z/z_w), \tag{4.1c}$$

$$\bar{u} - u_0 = A\{\tanh(z/z_w) - \{\tanh[(z - z_J - z_w)/z_J] + B\}(1 + B)^{-1}, \tag{4.1d}$$

where $B = \tanh[(z_J + z_w)/z_J]$ and A is defined so that the shear at the ground is unity. Equation (4.1a) is the familiar Charney profile, while (4.1b) is the piecewise linear finite depth shear zone considered in Held (1983). Profile (4.1c) is similar to (4.1b), save that the velocity approaches its asymptotic value smoothly. Profile (4.1d) is a jet with a peak wind near $z = z_w$ and which is asymptotic to the surface wind u_0 as $z \to \infty$. (See Table 1 for a schematic of these profiles.) The tropopause is modeled by setting $N = N_T$ for $z < z_T$ and $N = N_s$ for $z > z_T$.

If we introduce the transformed vertical coordinate

$$\zeta = \begin{cases} z, & z < z_T \\ z_T + \nu(z - z_T), & z \geqslant z_T, \end{cases} \tag{4.2}$$

where $\nu \equiv N_s/N_T$, and set $\eta = \rho_0^{1/2} v_\alpha$ then (2.3) again reduces to

$$(-\partial_{\zeta\zeta} + V)\eta = \lambda\eta \tag{4.3}$$

in nondimensional terms, where the potential is

$$V = \begin{cases} 1/4 - (r_0 + \bar{u}_z - \bar{u}_{zz})\bar{u}^{-1} + 2(\bar{u}_z\bar{u}^{-1} - 1/2)\delta(z), \\ \qquad\qquad z \leqslant z_T \\ (4\nu^2)^{-1} - [r_0 + \nu^{-2}(\bar{u}_z - \bar{u}_{zz})]\bar{u}^{-1}, \quad z \geqslant z_T, \end{cases} \tag{4.4}$$

and η_ζ has a jump at the tropopause given by

$$\eta_\zeta(z_T + \epsilon) = \nu\eta_\zeta(z_T - \epsilon) + \eta(z_T)\bar{u}(z_T)^{-1}[\nu\bar{u}_z(z_T - \epsilon) - \nu^{-1}\bar{u}_z(z_T + \epsilon) - (\nu - \nu^{-1})/2]. \tag{4.5}$$

Some qualitative features of the spectrum of eigenvalues can be discerned by examining the shape of the potential. In Fig. 8 we plot the potentials associated with profiles (4.1a), (4.1c) and (4.1d) for $u_0 = 0.214$, $r_0 = 0.5$, $z_w = 1.5$, $z_J = 0.5$ and $N_s = N_T$. The potentials for the Charney profile and the hyperbolic tangent profile resemble each other closely. For $z < 2.0$, V is slightly more negative for the hyperbolic tangent profile, owing to the effects of curvature of $\bar{u}$. In either case, the dominant features are a deep potential well below $z \approx 1.5$ and a repulsive δ-function at $z = 0$. The amplitude of the external mode will then increase away from the ground, attain a tropospheric peak, decrease toward an upper tropospheric turning point and patch into an exponentially decaying solution. The large z behavior of the two profiles differ in a noteworthy way, however, as shown in the insert in Fig. 8. For the Charney profile, as noted earlier, $V(\infty) = 0.25$ and $V - V(\infty) = -r_0/z$ at large z; thus the WKB phase integral (3.2) becomes infinite as $\lambda \to V(\infty)$, and the discrete spectrum of eigenvalues has an accumulation point at $V(\infty)$. For the hyperbolic tangent profile, the potential is asymptotic to -0.05, owing to the finite maximum wind. However,

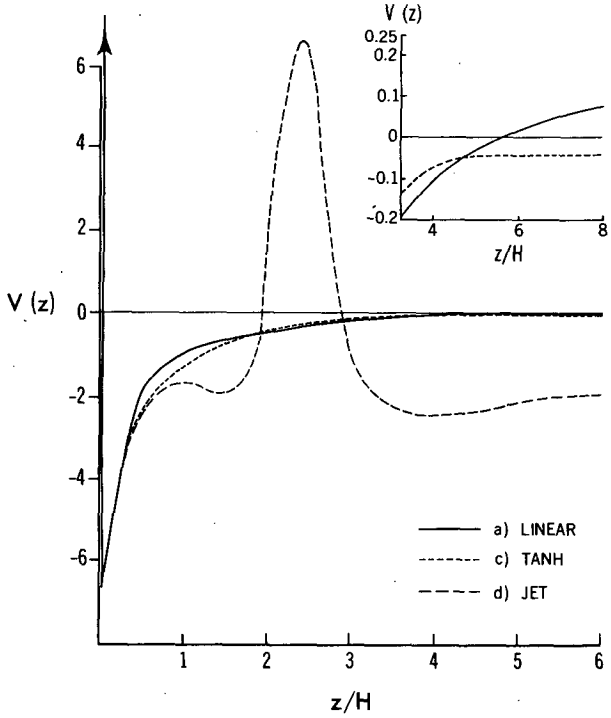

FIG. 8. The potential $V(z)$ given by (4.4) for the profiles (4.1a), (4.1c) and (4.1d). There is a repulsive δ-function at $z = 0$ in each case. The insert emphasizes the asymptotic behavior of the potential for the cases a) and c).

there is no accumulation point at $\lambda = -0.05$ because V approaches $V(\infty)$ exponentially, rendering the WKB phase integral finite. As z_w is made larger, the potential approaches the potential for the Charney profile over greater depths, and the number of horizontally wavelike discrete modes must eventually equal the number in Charney's model.

The potential for the jet profile differs substantially from those of the other two profiles. The curvature near the jet maximum deepens the potential markedly and the low value of $\bar{u}(\infty)$ makes $V(\infty)$ significantly negative. The potential well is separated from this flat portion by a pronounced potential barrier associated with the negative shear and positive curvature above the jet. This configuration is inimical to the existence of discrete modes. A discrete mode must have $\lambda < V(\infty)$ but λ must also be greater than the minimum value of V: since the δ-function at the origin is repulsive, we must have $\lambda > V(0+)$. This stringent restriction on λ limits the amount by which η can vary in the low-level propagating region and can render the matching to a rapidly decaying exponential in the potential barrier impossible. We will see below that this situation indeed occurs for the profile in question. However, it will also be seen that among the continuum of modes with $\lambda > V(\infty)$ the tropospheric response is very sharply peaked at a certain value of λ, leading to a tropospheric response that for all practical purposes is identical to that resulting from excitation of a discrete mode.

The discrete modes of the eigenvalue problem were obtained numerically using a variable step fourth-order Runge–Kutta routine to integrate (4.3) from the lower boundary to a height z_1 large enough that $\bar{u}$ could be considered uniform. The eigenvalue λ was adjusted with Newton's method until this solution matched smoothly onto the solution above z_1 with exponentially decaying energy.

We first turn to results for the hyperbolic tangent profile without a tropopause. Figure 9 shows the equivalent height z_e as a function of surface wind u_0 [or z_e/H as a function of $u_0/(\bar{u}_z(0)H]$ in dimensional terms) for $r_0 = 0.5$ and various values of z_w. In all cases shown, there is only one horizontally wavelike discrete mode for each u_0. We recall that for the Charney profile $z_e = 4/(r + 2) = 1.6$ at $u_0 = 0$, and $z_e = 1$ at large u_0. For $z_w = 3$, z_e is somewhat below the Charney profile result at small u_0, and approaches it more closely as u_0 increases. The value of z_e decreases with decreasing z_w and increases with decreasing u_0, but with a range of variation that becomes smaller as z_w is decreased. Thus, the infinite depth shear zone in the Charney profile leads to an overestimate of the equivalent height and of its sensitivity to the surface wind. In Fig. 9 we also show the corresponding results for the factor α_s useful in designing an equivalent barotropic model that predicts the correct wave amplitude. Recall that α_s reduces to unity when the traditional prescription of reducing the topography by the ratio of surface wind to model-level wind is used. With decreasing z_w, α_s decreases but remains larger than unity. The implication is that for a given surface wind and tropospheric wind shear,

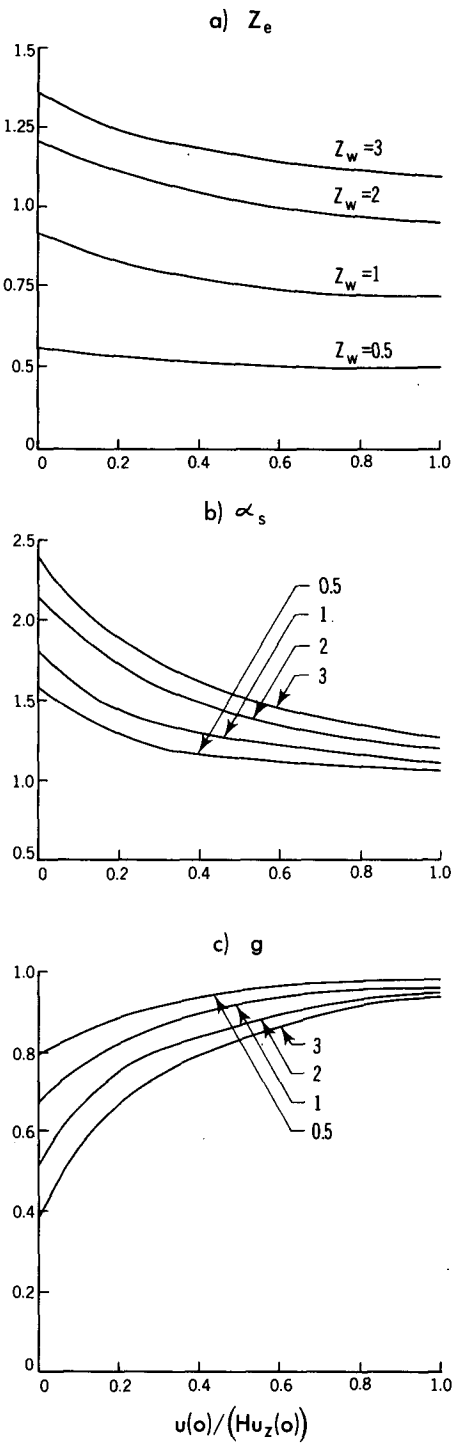

FIG. 9. z_e, α_s, and g as functions of u_0, for several values of z_w, for the hyperbolic tangent profile (4.1c), with $r_0 = 0.5$ and $N_s = N_T$.

the infinite depth shear zone in Charney's model results in an overestimate of the amplitude of the topographically forced external waves at z_e.

The final plot in Fig. 9 is of g, the ratio of barotropic group velocity to the group velocity of the external mode. Here we see an important difference between the results for the hyperbolic tangent profile and those for the Charney profile. The group velocities for the Charney profile become infinite as $u_0 \rightarrow 0$, whereas those for the hyperbolic tangent profile remain finite. The equivalent barotropic model still underestimates the true baroclinic group velocity, however, the discrepancy being greatest at small u_0 and large z_w.

In Table 1 we present the salient properties of the external mode for wind profiles (4.1a–d). The parameters are held fixed at $u_0 = 0.2141$, $z_w = 1.5$, $z_T = 1.5$, $z_J = 0.5$ and $r_0 = 0.5$. Results with a tropopause were computed using $(N_s/N_T)^2 = 2.5$; otherwise we set $N_s = N_T$. We show also the total stationary wavenumber $K = (-\lambda)^{1/2}$.

The addition of a tropopause is seen to have a minor effect on the results for the Charney profile, causing a slight shortening of the stationary wavelength and a slight decrease in the equivalent height. This insensitivity is in part due to the smallness of $\partial_z \bar{u}$ and $\partial_z \eta$ at the tropopause, since the jump in $\partial_z \eta$ at z_T [see (4.5)] is small as a result. A more notable consequence of the introduction of the tropopause into this particular basic state is that it leads to the existence of a second horizontally wavelike mode, a deep internal mode with $K = 0.093$. More will be said about this mode shortly. All other cases shown in Table 1 exhibit only a single horizontally wavelike mode.

The results for the piecewise linear profile and for the hyperbolic tangent profile are virtually identical, and in neither case does the tropopause have any appreciable effect. Evidently, it makes little difference whether the curvature is distributed, as in (4.1c), or gathered into a delta-function, as in (4.1b). In either case the wavelength is appreciably shortened and z_e, α_s, and g^{-1} are all reduced in comparison with the Charney profile. The shortening of the wavelength may be traced to the deepening of the potential by the flow curvature; the other changes are largely controlled by the wavelength shift.

The situation for the jet profile with $z_w = 1.5$ and $z_J = 0.5$ is rather different. No horizontally propagating discrete modes were found at $u_0 = 0.2141$ for this profile. In fact, a discrete mode did not appear until u_0 was made greater than 0.77. The configuration in Fig. 8 is similar to one in quantum theory which gives rise to a metastable state. In such a state, energy placed in the potential well is not completely trapped, but leaks out so slowly that the state has many features of a discrete mode. In pursuit of this idea, we examined continuum modes $v_m(z) = \rho_0^{-1/2}\eta_m$ normalized so that as $z \rightarrow \infty$, $v_m(z) \rightarrow (2/\pi)^{1/2} \times \cos(mz + \varphi)$, as required by (2.4). The mode index m ranges from zero to infinity and the phase shift $\varphi(m)$ is determined by integrating (4.3). According to (2.7) the topographically forced contribution of mode m evaluated at height z is proportional to $v_m(0)v_m(z)$. In Fig. 10 we show this quantity as a function of m [and of the corresponding $K(m)$] at height $z = 0.68$. This height is the equivalent height associated with the wavelength of maximum response (this particular jet profile produces an unrealistically low z_e), but the shape and width of the curve is virtually identical at all tropospheric altitudes. It is evident that the tropospheric response is dominated by a very narrow range of m (and hence of K). The width δK of the peak determines the downstream decay scale, as different waves in the continuum begin to destructively interfere only after a distance L such that $L\delta K > 1$. From the figure, we find $L \approx 50$ radii of deformation, whence we conclude that the downstream decay is negligible and that the tropospheric response is essentially the same as that due to a discrete mode with K set at the value of the peak response. We have not encountered any physically reasonable profiles for which metastability introduces appreciable decay, although the existence of such profiles has not been ruled out. In general, it seems that the curvature and shear above the jet act as an effective lid, and prevent significant leakage into the stratosphere. Values for K, z_e and α_s for the jet profile are included in Table 1.

Finally, we treat the question of the existence of multiple horizontally wavelike modes in the discrete spectrum. This problem will be addressed only for the hyperbolic tangent profile, so as to avoid the complications associated with computation of metastable states. Our goal is to identify the region of (u_0, z_w) space in which multiple wavelike modes exist. The shape of the region depends on r_0. Consider first

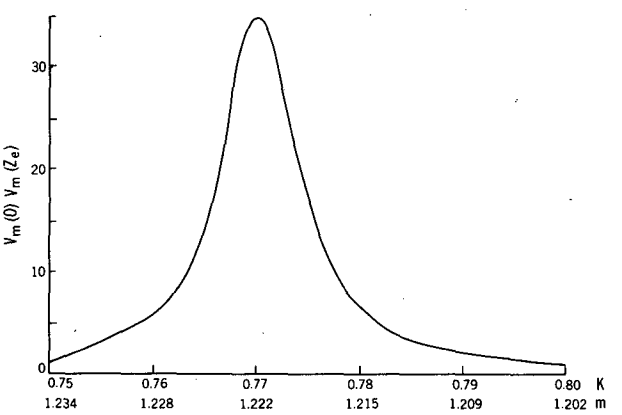

FIG. 10. The amplitude at the equivalent barotropic level of the continuum modes forced by topography for the jet profile (4.1d) as a function of the vertical wavenumber at infinity m, or horizontal wavenumber K, showing the peak corresponding to a metastable state.

$r_0 = 0.5$, for which the Charney profile has only a single wavelike mode. Without a tropopause, this was also found to be the case for the hyperbolic tangent profile, regardless of the value of z_w. With a tropopause of strength $(N_s/N_T)^2 = 2.5$ located at $z = 1.5$, a second mode enters at sufficiently large z_w. In Fig. 11a we show the region of (u_0, z_w) space in which a second mode exists. In terms of the transformed coordinate ζ, the high stratospheric static stability favors the existence of a second mode by deepening the region above the tropopause in which V is negative [see (4.2) and (4.4)]. It is then possible, for slightly negative λ, to fit an oscillation of η into the region above the tropopause and still match to a decaying exponential at the turning point. The jump condition (4.5) can also contribute by providing a discontinuous advance in the phase of the mode. Figure 11a shows that a second mode never exists for $z_w < 2.8$. For $z_w > 2.8$ there are very deep internal mode solutions corresponding to wave reflection from stratospheric winds. As such, they are qualitatively similar to the internal modes discussed by Plumb (1981) in connection with stratospheric sudden warmings. We note that increasing u_0 tends to suppress the second mode by making the potential everywhere shallower. Also, the folding of the boundary curve in Fig. 11a shows that increasing z_w can sometimes suppress the second mode. This is so because the curvature term deepens the potential but vanishes with increasing z_w.

In Fig. 11b we show the corresponding results for $r_0 = 1.5$ and $N_s = N_T$. At this value of r_0, the Charney profile without a tropopause permits a second mode as long as $u_0 < 1.6$ (see Fig. 5 or Fig. 6). For the hyperbolic tangent profile, a second mode exists only within certain ranges of z_w. For the case $u_0 \ll 1$ of most interest, a second mode exists when $z_w > 2.2$. As in the case $r_0 = 0.5$, the two-mode boundary folds over and approaches the critical u_0 for the Charney profile from the right.

Figure 11c shows the two- and three-mode boundaries for $r_0 = 1.5$ with a tropopause. These curves must also become vertical at large z_w; however, the asymptotic regime lies outside of the range of (u_0, z_w) plotted. For small surface winds, a second mode can exist when $z_w > 1.8$, a condition only slightly easier to satisfy than the corresponding condition for the no-tropopause case.

It thus appears that a second mode can exist only under conditions of weak shear extending over a deep layer. *Indeed, we find that if the shear extends only through* $\approx$*10 km* ($z_w \approx 1.5$) *then for a second mode to exist we must have* $r_0 > 2$ or, equivalently, shears less than ≈ 1 m s^{-1} km^{-1} (for $N^2 \approx 10^{-4}$ s^{-2} at 45°). As values of $r_0 > 2$ are rare in extratropical latitudes, the trapping of two modes below the tropopause must be viewed as very exceptional. Modes created by reflection from stratospheric or mesospheric winds may also occasionally play a significant role in tropospheric dynamics (see Tung and Lindzen, 1979; Plumb, 1981). However, with such high turning points, horizontal refraction and dissipation are much more likely to prevent the constructive interference between upward- and downward-propagating waves needed to create a modal structure.

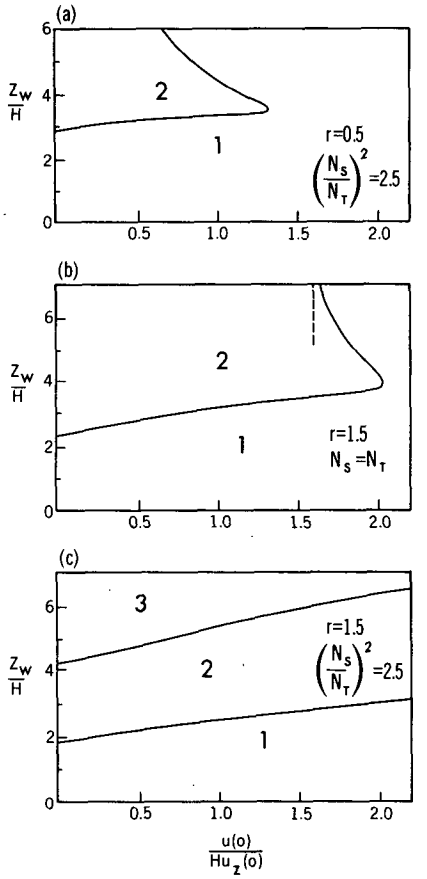

FIG. 11. Number of discrete horizontally propagating modes for the hyperbolic tangent profile (4.1c) as a function of nondimensional surface wind and z_w, for three different settings of the parameters r_0 and N_s/N_T.

5. Stationary external mode structures as a function of latitude

As a final calculation we consider a finite-differenced model with vertical resolution and upper boundary condition similar to that often used in general circulation models, and with basic state winds and static stabilities taken from observations. Encouraged by the qualitative success of ray tracing in explaining the structure of stationary waves in barotropic models linearized about zonal flows with realistic meridional structure, we calculate a *local* stationary wavenumber and vertical structure for the external mode by solving the following eigenvalue problem at each latitude θ:

$$f^2(\theta)\rho_0^{-1}\partial_z(\rho_0 N^{-2}\partial_z v_\alpha) + (\bar{u}a)^{-1}(\partial_\theta \bar{q})v_\alpha = -\lambda_\alpha v_\alpha$$
$$\bar{u}\partial_z v_\alpha = v_\alpha \partial_z \bar{u}, \quad z = 0 \quad \text{and} \quad z = z_T \qquad (6.1)$$

where

$$a^{-1}\partial_\theta \bar{q} \equiv \beta(\theta) + a^{-1}\partial_\theta \bar{\zeta} - f^2(\theta)\rho_0^{-1}\partial_z(\rho_0 N^{-2}\partial_z \bar{u}), \tag{6.2}$$

$$\bar{\zeta} \equiv -[a\cos(\theta)]^{-1}\partial_\theta[\bar{u}\cos(\theta)].$$

If the mean flow is sufficiently slowly varying with latitude, mode–mode coupling can be ignored, and a horizontal structure equation can be obtained for each mode, with $(-\lambda_\alpha)^{1/2}$ playing the role of the total horizontal wavenumber: $\lambda_\alpha = -k^2 - l^2$. As before, a requirement for horizontal propagation is that $\lambda_\alpha < 0$. Setting $m \equiv ka\cos(\theta)$ and

$$m_\alpha^2 \equiv -\lambda_\alpha a^2 \cos^2(\theta), \tag{6.3}$$

the wavenumber m component of mode α will be meridionally propagating only in those regions where $m^2 < m_\alpha^2$.

We compute $\bar{u}^{-1}\partial_\theta \bar{q}$ and N^2 at 5° intervals from the Northern Hemisphere wintertime climatology in Oort and Rasmussen (1971), using standard centered finite-differencing, and restricting the calculation to those latitudes (30°, ..., 65°) at which $\bar{u} > 0$ at all levels. Data is provided at eleven pressure levels (1000, 950, ..., 100, 50 mb). Standard centered finite-differencing is also used for (6.1), using the same vertical levels at which the data is given. The finite-differenced boundary conditions are

$$(\bar{u}_1 + \bar{u}_2)(v_{\alpha,1} - v_{\alpha,2}) = (\bar{u}_1 - \bar{u}_2)(v_{\alpha,1} + v_{\alpha,2}),$$

where the subscripts (1, 2) correspond to (950, 1000) mb for the lower boundary condition and (50, 100) mb for the upper. With this finite-differencing, the eigenvalue problem yields nine discrete modes. *At each latitude we find that one and only one mode is horizontally wavelike* ($K_e^2 = -\lambda_e > 0$), just as in Charney's model when $r < 1$. We have repeated this calculation with summertime data and once again obtain only one wavelike mode, except at one latitude near the subtropical transition from surface westerlies to easterlies. Thus, in nearly all cases examined, vertical finite-differencing comparable to that used in many GCMs does not introduce spurious horizontally wavelike modes. This is not to say that such spurious modes can never be produced. For example, if one takes the tanh profile (4.1c) and places a rigid lid at a sufficiently high altitude, spurious horizontally wavelike modes can always be created, whether the model is continuous or finite-differenced. In models which extend to the tropopause or only slightly beyond, however, there is insufficient room in the vertical to fit these modes.

The vertical structure of the geopotential for this external mode is shown in Fig. 12 for 30, 45 and 60°. In each case the structure is broadly similar to that of the external mode in Charney's model (see Fig. 4). One finds that these small differences in vertical structure at different latitudes do not suffice to explain the observed latitudinal dependence in the

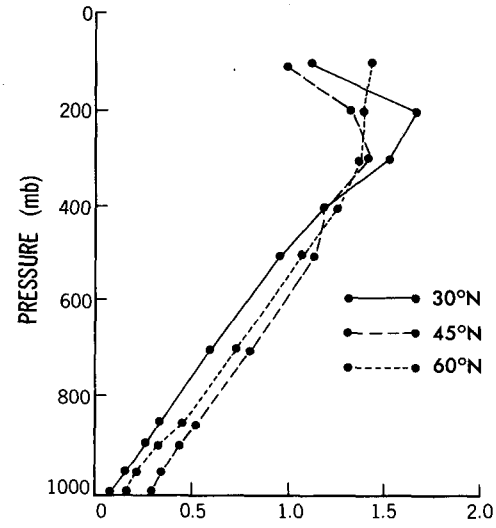

FIG. 12. Vertical structure of the stationary external mode geopotential in the finite-differenced model described in the text, using observed Northern Hemisphere zonal winds and static stabilities, at three different latitudes.

vertical structure of the *zonally averaged* stationary eddy geopotential variance in Northern Hemisphere winter. The baroclinic "near-field" responses (see Fig. 2) evidently complicate the picture.

The vertical structures in Fig. 12 do bear a striking resemblance to the mean zonal wind profiles. In fact, the small differences between the three curves in the figure are qualitatively similar to differences between the zonal flows at these latitudes. The following scaling argument helps one understand this similarity, thereby providing an alternative way of understanding the maximum in amplitude in the upper troposphere. The stationary external Rossby wavelength is generally significantly larger than the radius of deformation NH/f, while the vertical "scale" of the mode, $v_e(\partial_z v_e)^{-1}$, is larger than H throughout much of the troposphere, so the usual quasi-geostrophic scaling implies that the effects of vertical motion in the temperature equation are modest. Therefore, $v_e\partial_z\bar{u} \approx \bar{u}\partial_z v_e$ or $v_e \approx \bar{u}$; in particular, the maximum in meridional velocity (or geopotential) should be near the maximum in $\bar{u}$. Nonlinear equivalent barotropic models, in which the *total* flow is assumed to be separable, have played an important historical role in numerical weather prediction. The utility of such models is evidently a consequence of this similarity in vertical structure between stationary (or quasi-stationary) external modes and the mean flow on which they propagate. The results for Charney's model in the limit of small surface winds described in Section 3 help one appreciate the limitations of this scaling argument. In that case, $\bar{u} \propto z$ while $v_e \propto z\exp[-rz/(2H)]$, so that $v_e \approx \bar{u}$ over more than a scale height only if the vertical shear is sufficiently large that $r \ll 1$, resulting in a stationary wavenumber that is much smaller than $f/(NH)$.

The equivalent barotropic pressure p_e, at which $\bar{u} = (\beta + a^{-1}\partial_\theta\zeta)K_e^{-2}$, obtained by linearly interpolating in $\ln(p)$, is shown as a function of latitude at the top of Fig. 13. In all cases, p_e lies between 400 and 450 mb. This is somewhat lower than what one would estimate based on Charney's model. The corresponding value of m_e [Eq. (6.3)] is also shown (cf. the analogous plot for a barotropic model in Hoskins and Karoly, 1981, Fig. 13b). One can infer from this figure, for example, that a wavenumber 4 external mode can only propagate equatorward of ~55°. The fact that m decreases with increasing latitude implies that all rays are ultimately refracted into the tropics. Using this climatological zonally averaged basic state, there is no hint of a minimum in m that would raise the possibility of extratropical trapping. We emphasize that this does not rule out the possibility of trapping at certain times and in certain longitudinal sectors.

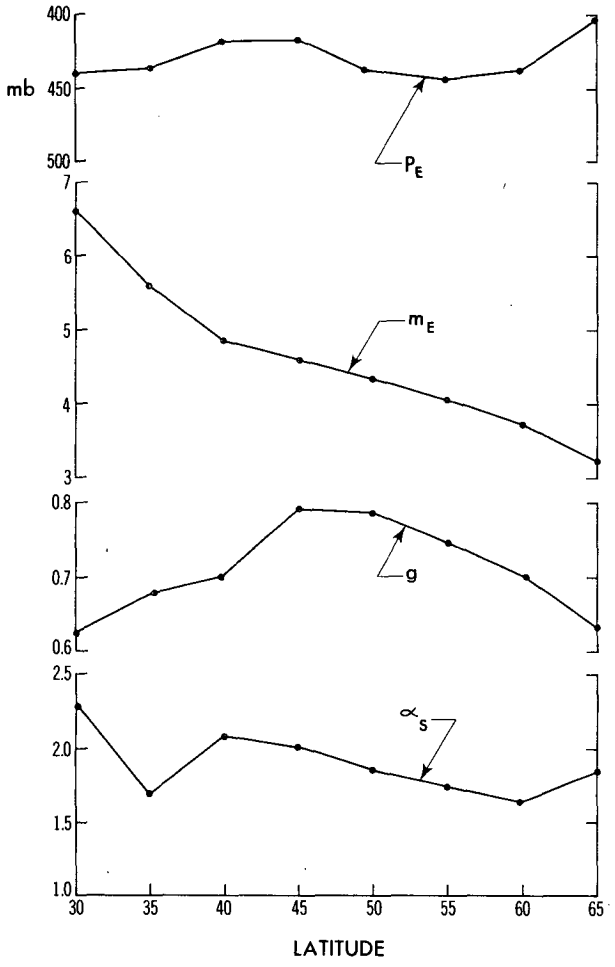

FIG. 13. Properties of the stationary external mode [p_e = equivalent barotropic pressure; m_e = zonal wavenumber dividing meridionally propagating ($m < m_e$) and trapped ($m > m_e$) waves; g, see (2.27); and α_s, see (2.15)] as functions of latitude in the finite-differenced model with observed Northern Hemisphere wintertime winds and static stabilities.

Also shown in Fig. 13 are the group velocity ratio g and the surface wind amplification factor α_s. As expected from the results of the previous sections, g is considerably less than unity, ranging from 0.6 to 0.8, implying that an external mode wavetrain propagates faster than a wavetrain in the corresponding equivalent barotropic model. The plot of α_s shows that surface winds must be multiplied by roughly a factor of 2 before being blown over the topography to obtain the correct vorticity source for use in an equivalent barotropic model.

All of the results in Fig. 13 are insensitive to modest changes in the low-level wind field, such as increasing the winds in the lowest two or three levels by a few m s^{-1}. This is encouraging, since the observed winds are affected by boundary layer stresses, and it is unclear which winds are appropriate for use in an inviscid analysis. There are other quantities of interest that *are* sensitive to small changes in low-level winds, the most important being α, that is, the actual amplitude of the far-field wave [see (2.14)]. Sensitivity of the wave amplitude to low-level winds is unavoidable in a linear theory in which the topographic forcing vanishes as $\bar{u}(0) \to 0$. The value of g_{Ek} [Eq. (2.31)] is also found to be sensitive to the details of the low-level winds.

6. Conclusions

The typical planetary-scale response to a localized stationary midlatitude source consists of a packet of long Rossby waves that propagates into the stratosphere and a packet of shorter Rossby waves trapped between the upper tropospheric westerlies and the surface. The latter packet rapidly takes on the vertical and horizontal structure of the stationary external mode, with maximum geopotential amplitude near the tropopause and relatively small amplitude near the surface. It is this vertical structure that dominates much of the stationary eddy pattern in midlatitudes. That stationary eddy patterns are equivalent barotropic to a considerable degree is explained by the fact that the external mode is nearly always the only stationary wave trapped in the troposphere, and must therefore dominate the tropospheric response far from the source. While it is possible to trap more than one stationary mode within the troposphere, this requires smaller shears than are generally observed, as shown in Sections 3 and 4.

The vertical structure of equivalent barotropic low-frequency transients, such as the PNA teleconnection pattern, can be explained in precisely the same way. While the nonlinear cascade of energy to larger vertical, as well as horizontal, scales may play some role in exciting these patterns and nonlinearity may be important for their persistence and decay, we see no need to invoke nonlinearity to explain the observed vertical structure.

In a model with a rigid-lid upper boundary condition and finite-differencing with resolution typical

of GCMs, and using observed wintertime zonal winds and static stabilities, we again find the external mode to be the only horizontally wavelike stationary mode, in agreement with continuous, semi-infinite models. If this were not the case, we suspect that the tropospheric stationary wave field in such models would be seriously distorted.

If the zonal flow is independent of latitude or, more realistically, if the meridional variations are sufficiently slow that mode–mode coupling can be ignored, then that part of the forced response due to the external mode satisfies the stationary barotropic vorticity equation linearized about a mean flow u_e. The equivalent barotropic height, z_e, at which $\bar{u} = u_e$, depends on the structure of the mean flow. In the linear shear flow $\bar{u} = u_0 + \Lambda z$, z_e is $4H/(2 + r)$ when $u_0 \ll \Lambda H$, where H is the scale height and $r = \beta N^2 H/(f_0^2 \Lambda)$; it is $\approx$425 mb in the calculations with observed mean winds in Section 5. For topographic forcing, the vortex tube stretching to be used in an equivalent barotropic model so as to predict the correct far-field response at z_e is typically overestimated by blowing the equivalent barotropic wind u_e over the topography and dividing by the scale height, and underestimated (by roughly a factor of 2, according to the results of Section 5) by replacing u_e with $\bar{u}(0)$.

The group velocity of stationary external Rossby waves is generally larger than the group velocity of stationary waves of the same wavelength in a barotropic model. The linear shear flow has the peculiar property that the group velocity of stationary external waves tends to infinity as $\bar{u}(0)$ tends to 0, if one ignores the very small non-Doppler term in the lower boundary condition. For more realistic wind profiles, the group velocity increases, but remains finite, as $\bar{u}(0) \to 0$.

When the winds above the tropospheric jet decrease to small values and remain small with increasing height, there may be no true stationary discrete vertical modes at all. However, in the cases we have examined of this type, there always exists a metastable state for which leakage into the stratosphere is so small that it results in negligible downstream decay of the stationary wavetrain. A transition to easterlies in the stratosphere would also eliminate any possibility of a true linear discrete stationary mode. Although the discussion in this paper has been restricted to the case of westerly mean winds, one can anticipate that such a critical level would not destroy the physical importance of the external mode, but once again introduce some downstream decay.

Acknowledgments. We would like to thank Y. Hayashi and M. Salby for helpful reviews of the manuscript. RLP acknowledges support from NOAA Grant 04-7-022-44017.

APPENDIX

Derivation of Equation (2.29)

A relation between $\partial K_e^2/\partial u_0$ and the vertical structure of the external mode can readily be obtained from the eigenvalue problem in the form (2.24). Replacing u_0 with $u_0 + \delta u_0$ results in the perturbed potential $V + \delta V$, where

$$\delta V = \bar{u}^{-2}\delta u_0[\epsilon\bar{q}_y - 2\partial_z\bar{u}\delta(z)], \tag{A1}$$

and $\epsilon(z) \equiv (N/f_0)^2$. The perturbed external mode eigenvalue is then

$$\delta K_e^2 = -\delta\lambda_e = -\int_0^\infty \eta_e^2 \delta V dz \Big/ \int_0^\infty \epsilon\eta_e^2 dz. \tag{A2}$$

Once again using the normalization

$$H^{-1}\int_0^\infty N^2\eta_e^2 dz = \langle v_e^2\rangle = 1, \tag{A3}$$

where $v_e = \rho_0^{-1/2} N\eta_e$, we have

$$\begin{aligned}-\partial K_e^2/\partial u_0 &= \langle v_e^2\bar{u}^{-2}(q_y - \epsilon^{-1}\partial_z\bar{u})\rangle \\ &= K_e^2\langle v_e^2\bar{u}^{-1}\rangle + f_0^2\langle N^{-2}(\partial_z v_e)\partial_z(v_e\bar{u}^{-1})\rangle.\end{aligned} \tag{A4}$$

The second expression in (A4) is obtained by using the relations

$$\bar{u}(-K_e^2 v_e + f_0^2\rho_0^{-1}\partial_z(\rho_0 N^{-2}v_e) = -\bar{q}_y v_e, \tag{A5}$$
$$\bar{u}\partial_z v_e = v_e\partial_z\bar{u}, \quad z = 0.$$

Substitution into (2.27) then yields the expression (2.29) for g.

REFERENCES

Blackmon, M. L., R. A. Madden, J. M. Wallace and D. S. Gutzler, 1979: Geographical variations in the vertical structure of geopotential height fluctuations. *J. Atmos. Sci.*, **36**, 2450–2466.

Bretherton, F. P., 1966: Critical layer instability in baroclinic flows. *Quart. J. Roy. Meteor. Soc.*, **92**, 325–334.

Burger, A. P., 1962: On the existence of critical wavelengths in a continuous baroclinic stability problem. *J. Atmos. Sci.*, **19**, 31–48.

Charney, J. G., 1947: The dynamics of long waves in a baroclinic westerly current. *J. Meteor.*, **4**, 135–162.

——, and A. Eliassen, 1949: A numerical method for predicting the perturbations of the midlatitude westerlies. *Tellus*, **1**, 38–54.

Dole, R. M., 1983: Persistent anomalies of extratropical Northern Hemisphere wintertime circulation. *Large-Scale Dynamical Processes in the Atmosphere*, B. Hoskins and R. Pearce, Eds., Academic Press, 95–109.

Friedman, B., 1966: *Principles and Techniques of Applied Mathematics*, Wiley and Sons, 315 pp.

Geisler, J. E., and R. E. Dickinson, 1975: External Rossby waves on a beta-plane with realistic vertical wind shear. *J. Atmos. Sci.*, **32**, 2082–2093.

——, and ——, 1976: The five-day wave on a sphere with realistic zonal winds. *J. Atmos. Sci.*, **36**, 223–234.

Gill, A. E., 1983: *Atmosphere-Ocean Dynamics,* Academic Press, 662 pp.

Grose, W. L., and B. J. Hoskins, 1979: On the influence of orography on large-scale atmospheric flow. *J. Atmos. Sci.,* **36,** 223–234.

Held, I. M., 1983: Stationary and quasi-stationary eddies in the extratropical troposphere: Theory. *Large-scale Dynamical Processes in the Atmosphere,* B. Hoskins and R. Pearce, Eds., Academic Press, 127–168.

——, R. T. Pierrehumbert and R. L. Panetta, 1985: Dissipative destabilization of external Rossby waves. *J. Atmos. Sci.,* (in press).

Holton, J. R., 1979: *An Introduction to Dynamical Meteorology,* 2nd ed., Academic Press, 391 pp.

Hoskins, B. J., and D. J. Karoly, 1981: The steady linear response of a spherical atmosphere to thermal and orographic forcing. *J. Atmos. Sci.,* **38,** 1179–1196.

——, and R. Pearce, Eds., 1983: *Large-scale Dynamical Processes in the Atmosphere,* Academic Press, 397 pp.

Lindzen, R. S., 1967: Planetary waves on a beta-plane. *Mon. Wea. Rev.,* **95,** 441–451.

Namais, J., 1978: Multiple causes of the North American winter 1976–77. *Mon. Wea. Rev.,* **106,** 279–295.

Oort, A. H., and E. M. Rasmussen, 1971: Atmospheric Circulation Statistics. NOAA Prof. Paper 5, U.S. Dept. of Commerce, Washington, DC, 323 pp.

Panetta, R. L., I. M. Held and R. T. Pierrehumbert, 1985: A note on stationary external Rossby waves in the two layer model. (In preparation).

Pedlosky, J., 1979: *Geophysical Fluid Dynamics.* Springer-Verlag, 624 pp.

Plumb, R. A., 1981: Instability of the distorted polar night vortex: A theory of stratospheric warmings. *J. Atmos. Sci.,* **38,** 2514–2531.

Randel, W. J., and J. L. Stanford, 1983: Structure of medium-scale atmospheric waves in the Southern Hemisphere summer. *J. Atmos. Sci.,* **40,** 2312–2318.

Salby, M. L., 1981: Rossby normal modes in nonuniform background configurations. Part 1: Simple fields. *J. Atmos. Sci.,* **38,** 1803–1826.

Simmons, A. J., 1982: The forcing of stationary wave motion by tropical diabatic heating. *Quart. J. Roy. Meteor. Soc.,* **108,** 503–534.

Tung, K. K., and R. S. Lindzen, 1979: A theory of stationary waves in the presence of realistic vertical shears. *Mon. Wea. Rev.,* **107,** 735–750.

Wallace, J. M., 1983: The climatological mean stationary waves: Observational evidence. *Large-scale Dynamical Processes in the Atmosphere,* B. Hoskins and R. Pearce, Eds., Academic Press, 27–53.

——, and D. S. Gutzler, 1981: Teleconnections in the geopotential height field during the Northern Hemisphere winter. *Mon. Wea. Rev.,* **109,** 785–812.